

Inland ship stern optimization in shallow water

Rotteveel, Erik; Hekkenberg, Robert; van der Ploeg, Auke

DOI

[10.1016/j.oceaneng.2017.06.028](https://doi.org/10.1016/j.oceaneng.2017.06.028)

Publication date

2017

Document Version

Final published version

Published in

Ocean Engineering

Citation (APA)

Rotteveel, E., Hekkenberg, R., & van der Ploeg, A. (2017). Inland ship stern optimization in shallow water. *Ocean Engineering*, 141, 555-569. <https://doi.org/10.1016/j.oceaneng.2017.06.028>

Important note

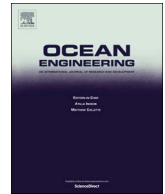
To cite this publication, please use the final published version (if applicable). Please check the document version above.

Copyright

Other than for strictly personal use, it is not permitted to download, forward or distribute the text or part of it, without the consent of the author(s) and/or copyright holder(s), unless the work is under an open content license such as Creative Commons.

Takedown policy

Please contact us and provide details if you believe this document breaches copyrights. We will remove access to the work immediately and investigate your claim.



Inland ship stern optimization in shallow water



Erik Rotteveel^{a,*}, Robert Hekkenberg^a, Auke van der Ploeg^b

^a Delft University of Technology, 3mE, Mekelweg 2, 2628CD Delft, The Netherlands

^b Maritime Research Institute Netherlands, Haagsteeg 2, 6708PM Wageningen, The Netherlands

ARTICLE INFO

Keywords:

Ship propulsion power
Shallow water
Restricted water
Inland ships
Hull form optimization
Surrogate modeling

ABSTRACT

Inland ships continuously operate in restricted waters, where the depth and width are regularly less than twice the ship's draft and four times ship breadth, respectively. In restricted water, the flow around the hull changes compared to that in unrestricted water due to presence of the fairway bottom and sides, that lead to increased return flow, stronger squat effects and changes in the wave pattern produced by the ship. If these changes to the flow are significant, it is worthwhile to optimize the hull form for shallow or confined water rather than for unrestricted water. This paper specifically focuses on the effects of water depth on inland ship stern optimization. It presents the optimization of propulsion power for various water depths using a parametric inland ship stern shape, CFD and surrogate modeling. The change of parameter influence in different water depths is analyzed and explained by means of flow visualization. Using Pareto fronts, a trade-off is shown: propulsion power in shallow water can be decreased at the cost of increased propulsion power in deep water and vice versa.

1. Introduction

If a ship navigates in shallow water, its resistance will increase compared the resistance in deep water. Multiple methods have been proposed to estimate the magnitude of this increase (Schlichting, 1934; Lackenby, 1963; Tuck, 1978; Ferreiro, 1992; Raven, 2016). Apart from resistance, which has a direct effect on the required propulsion power, the wake fraction and thrust deduction will also change (Rotteveel and Hekkenberg, 2015; Raven, 2012). The propeller open water efficiency also changes due to different propeller loading (Harvald, 1977). Propulsion power is thus affected in multiple ways.

These changes follow from a combination of differences in the flow compared to that in deep water. In shallow water, less water can pass the ship underneath, leading to increased return flow speed. Also, motions in the flow are limited in vertical direction forcing the flow to follow a more horizontal trajectory around the hull. Furthermore, the increased return flow speed causes lower pressures underneath and around the hull. This leads to additional sinkage, water level depression around the ship and typically increased wave resistance (in some cases it may decrease, see (Raven, 2016)).

Especially effects that change the trajectories of the fluid around the ship require that the hull form is adapted to the flow in shallow water to achieve minimal power required for propulsion. Whereas this might not be important for sea-going vessels that only encounter shallow water on a very limited basis, inland ships encounter shallow water

continuously during navigation, with depth-to-draft (h/T) ratios often being lower than 2.0. We will therefore investigate whether, and to what extent, an inland ship hull form should be optimized for shallow water rather than for deep water. Optimization studies for wave resistance in shallow water have been published (Zhao, 1984; Saha et al., 2004), but given the changes to wake fraction, thrust and propeller efficiency, propulsion power should be addressed during optimization for shallow water.

This paper discusses the propulsion power optimization of a parametric inland ship stern including four parameters: the athwartships propeller position, the tunnel-top curve, the bottom plane shape and the stern bilge radius. Double-body CFD (Computational Fluid Dynamics) calculations are used to estimate the power requirement of the ships varied with these four parameters at four different water depths ($h/T = 3.0, 2.0, 1.5$ and 1.2). A surrogate model is generated from the results, the type of which is selected based on model convergence and cross-validation. Multi-objective optimization is then performed using these surrogate models, for which the objective functions are the power estimates at different water depths. The Pareto front resulting from the optimization is then investigated to see which parameters change if a different water depth is selected to optimize for.

The next section discusses the approach. It includes the applied parameters, CFD method and result analysis method. Section 3 shows the results of response surface investigation, certain CFD results and

* Corresponding author.

E-mail address: e.rotteveel@tudelft.nl (E. Rotteveel).

Nomenclature

B	Ship width, m	R_T	Total resistance (with propeller), N
C	Bernoulli-constant, –	S	Submerged surface area, m^2
Cd	Resistance coefficient, –	t	Thrust deduction factor, –
C_p	Dynamic pressure coefficient, –	T	Ship draft, m
g	Gravitational constant, 9.81 m/s^2	u^x	x -component of velocity vector, m/s
h	Water depth, m	V_S	Ship speed, m/s
L_{pp}	Ship length, m	w_E	Effective wake fraction, –
p	Pressure, N/m^2	w_N	Nominal wake fraction, –
p_h	Hydrostatic pressure, N/m^2	w_T	Total wake fraction, –
P_D	Propulsion power, kW	x, y, z	Coordinates, m
r	Radial coordinate on propeller disk, m	Δp	Pressure jump at propeller disk, N/m^2
R	Propeller radius, m	η_O	Propeller open-water efficiency, –
R_N	Nominal resistance (without propeller), N	η_R	Relative rotative efficiency of propeller, –
		η_H	Hull efficiency, –
		ρ	Water density, kg/m^3

the Pareto fronts obtained during the optimization. Section 4 presents an analysis and discussion of the results while Section 5 contains an overview of the conclusions along with recommendations for further research.

2. Approach

2.1. Reference hull form

This investigation focuses on the stern of an inland ship. The stern of the used reference hull form is shown in Fig. 1, with the waterline indicated by the blue line. The length, beam and draft of the ship are 110.00, 11.40 and 3.50 m respectively, which correspond to a typical European Class Va inland ship. Fig. 1 includes a free board height of 1.5 m, which is not modeled in the double-body CFD calculations.

Fig. 1 includes the stern tunnel geometry. Such a tunnel is commonly applied to inland ships to prevent propeller ventilation at low draft, which occurs in case the ship is empty, partially loaded or if the ship cannot be fully loaded if the draft is limited due to a low water depth. The propeller is then close to the water surface, increasing the risk of propeller ventilation which leads to a large loss of thrust. Although the tunnel prevents this, the skirts as shown in Fig. 1 should be carefully designed to align it with the flow around the hull in order to minimize resistance.

2.2. Hull form parameters

The hull form (Fig. 1) is varied based on four parameters. Fig. 2 shows how each of the parameters affects the ship frames. The first, Y_{prop} , affects the lateral propeller position. Next, V_{bottom} changes the shape of the flat-of-bottom from V-Shaped to S-Shaped. R_{bilge} affects the bilge radius in the stern and V_{top} changes the curvature of the tunnel top curve (i.e. a curve that can be drawn through the highest point in every tunnel frame). This curve is either aligned with the tunnel Skirt (see Fig. 1), or is S-Shaped such that it ends in a longitudinal direction at the propeller plane. For a clean lay-out of graphs, we will use V1, V2, V3 and V4 for Y_{prop} , V_{bottom} , R_{bilge} and V_{top} respectively.

2.3. Experiment design

The parameters are varied using a Latin Hypercube (LH) (Sacks et al., 1989) experiment design with 50 design points. A LH design is a space-filling design such that the design points are spread equally across the design space. This ensures that there is no clustering of points in a certain region of the design space, which would have other regions not adequately covered. Furthermore, a LH design furthermore requires less computations to be conducted than a full factorial grid (in

which all parameters are varied in an equal number of steps, with equal step size), saving computational time while still obtaining sufficient information on the effects of variations. Each of the hull forms is subject to four different h/T ratios: $h/T = 3.0, 2.0, 1.5$ and 1.2 , corresponding to water depths of $h = 10.5, 7.0, 5.25$ and 4.2 m. After performing the computations, 8 ships had to be removed from the data set since the corresponding CFD calculations diverged, yielded non-physical results or because the obtained results were far off the global trends. The removed points were randomly spread across the design space. Also, randomly removing even more results (up to 10), does not affect the analysis of the dataset significantly.

2.4. CFD approach

The ship hull forms are generated using a parametric model built in Rhinoceros 3D. The hull form surface is then discretized into a wall grid using Rhino plug-ins developed at MARIN (Maritime Research Institute Netherlands). The flow around each hull form is computed using Parnassos (Hoekstra, 1999), a Reynolds-Averaged Navier-Stokes (RANS) solver developed at MARIN and IST (Instituto Superior Técnico). This code uses multi-block, structured, body-fitted grids that are generated by means of solving Laplace equations. A strong contraction of the grid is applied towards the hull surface, which together with a specific solution strategy offers the solution of the boundary layer flow without using wall functions. A one-equation turbulence model is applied (Menter, 1997). Furthermore, the solver uses a downstream marching scheme solving the flow in downstream propagating blocks rather than solving the whole domain at once. This leads to an efficient solving procedure (Van der Ploeg et al., 2001) making the code very suitable for systematic evaluations while obtaining results in good agreement with experimental data (Van der Ploeg and Starke, 2013).

For the present study, steady double-body calculations are applied.

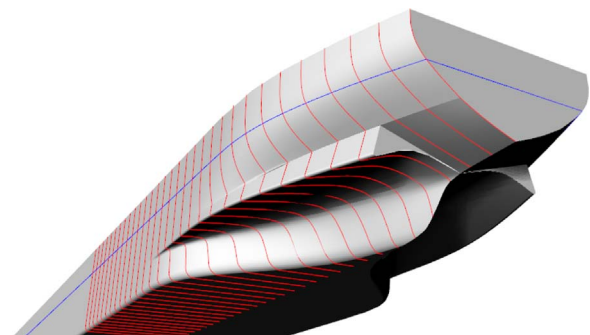


Fig. 1. Overview of the stern hull of the used inland ship. The tunnel skirt to prevent propeller ventilation is shown as well as the tunnel geometry.

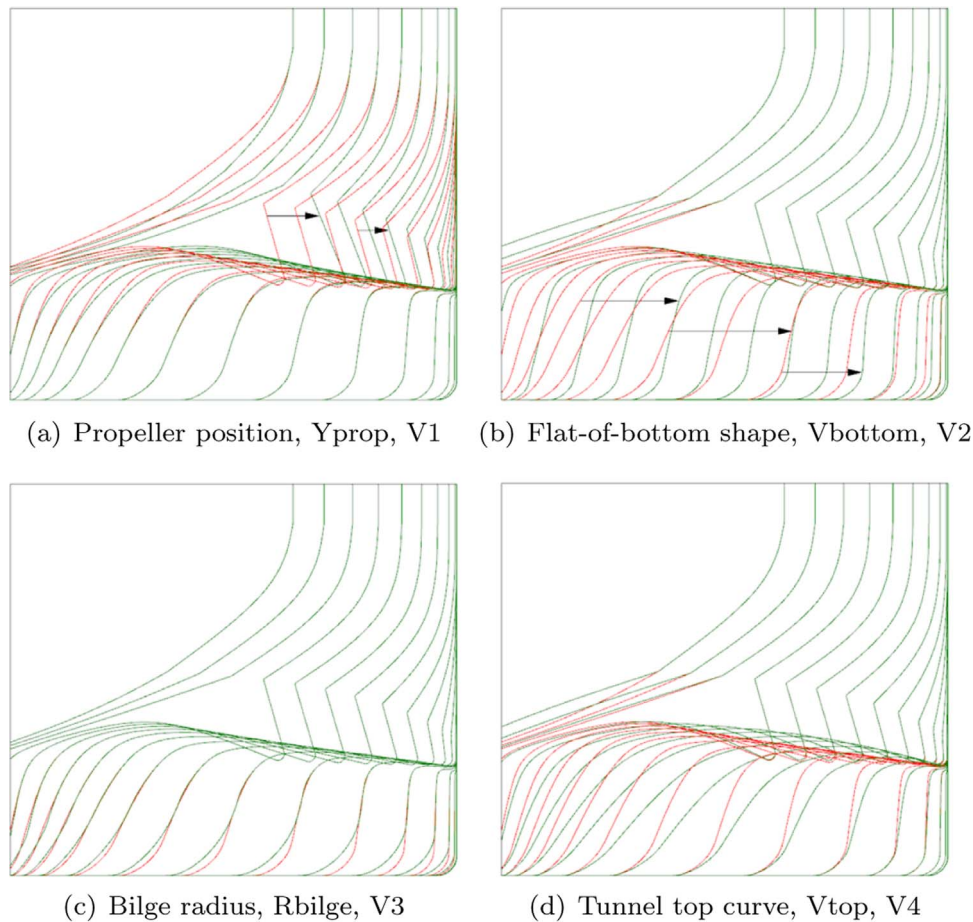


Fig. 2. Overview of variations applied to stern hull.

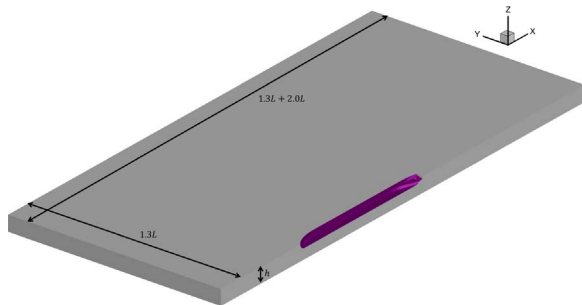


Fig. 3. Overview of the computational domain, with dimensions for domain width and length. The height of the domain depends on the water depth h for the current calculation.

Double-body calculations do not allow for the estimation of wave resistance, which generally increases in shallow water. However, the investigated hull form parameters only affect the submerged part of the stern. Furthermore, inland ships operate at relatively low Froude numbers. Therefore, the interaction between increased wave resistance and trends with respect to the stern shape parameters is limited.

The effect of the propellers on the flow is modeled by applying a distribution of body forces in the flow field. For the present study, a circular-symmetric force distribution is used. Only forces in x -direction are applied, tangential and radial forces are zero. The force in x -direction depends on the radial position such that the maximum thrust force is applied at $r/R = 0.7$, with R being the propeller radius and r the distance from the propeller shaft.

The computational domain extends to $1.3L_{pp}$ upstream of midship, $2.0L_{pp}$ downstream of midship and $1.3L_{pp}$ sideways (far-field). Fig. 3

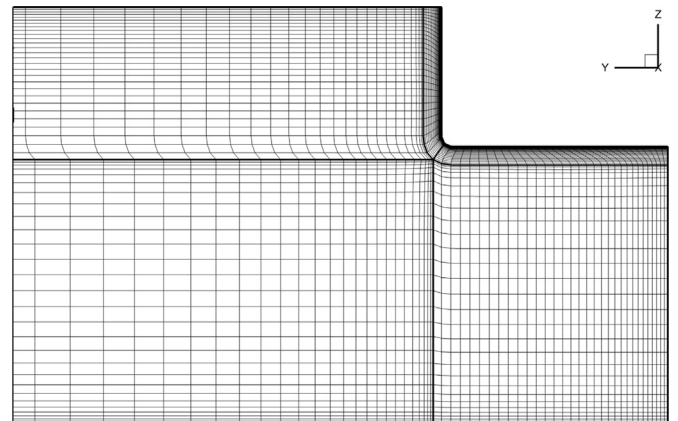


Fig. 4. Overview of the five-block structured grid around midship. The ship is located in the top right of the figure, the grid contraction towards the hull is presented as well. On the left, the grid extends up to $y = 1.3L_{pp}$.

shows the computational domain for $h/T = 3.0$. At the inflow boundary, velocity is fixed to the ship speed. At the outflow boundary, the pressure gradient in x -direction is zero. Tangential velocities and pressures at the far-field boundary are fixed based on results of potential flow calculations. Furthermore, a no-slip conditions is applied at the ship hull and a moving no-slip wall is applied at the fairway bottom. Finally, symmetry conditions are used at the free-surface and at the ship center plane ($y = 0$).

The mesh around the parallel midship is presented in Fig. 4. For shallow water calculations, a five-block grid is used, since the number of boundaries in a transverse plane is five and a structured grid only

Table 1

Resistance coefficients values for different grids. The relative cell size is measured against that for the grid used for the present study. For the present grid, the estimated numerical uncertainty is 1.6.

Relative cell size	Resistance coefficient
1.67	2.663E-3
1.43	2.685E-3
1.25	2.699E-3
1.11	2.696E-3
1.00	2.719E-3
0.91	2.705E-3
0.83	2.725E-3

Table 2

Comparison of nominal and effective wake fractions at different h/T ratios for a specific ship that was analyzed.

h/T	w_N	w_E
3.0	0.182	0.128
2.0	0.210	0.150
1.5	0.259	0.178
1.2	0.446	0.237

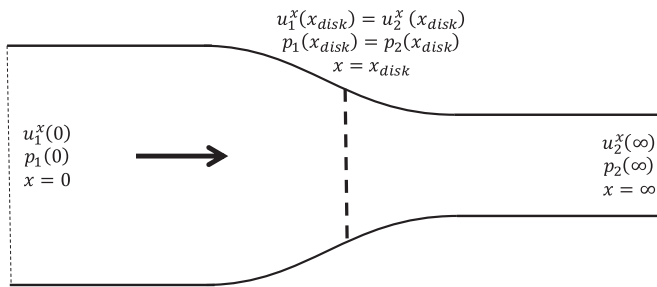


Fig. 5. Schematic overview of flow through propeller disk with the symbols used in Eqs. (2), (3) and (4).

has four sides. Fig. 4 also shows the strong grid contraction towards the hull. In all computations, y^+ values are well below 1.0. A grid-dependence study has been conducted with 7 grids. 2 of these grids counted consist of smaller cells than the reference grid (which has been used for the present study). 4 grids have coarser cells. The resistance coefficients per grid are given in Table 1. Since precise geometrical equivalence is difficult to obtain, the procedure proposed in (Eca and Hoekstra, 2014) is applied. From this procedure, a numerical uncertainty of 1.6 percent was estimated for the grids used in the present study.

2.5. Power estimation

From the flow solution obtained using Parnassos, the resistance of the ship, wake field and thrust deduction are determined. Thrust deduction is obtained from conducting calculations without and with the propeller effect as described in the previous section. These are respectively called a nominal and a total calculation. From resistance, the thrust deduction factor and the wake field, an estimate of propulsion power is obtained as follows:

$$P_D = \frac{R_N \cdot (1 - w_E)}{1 - t} \cdot \frac{V_S}{\eta_O \eta_R} \quad (1)$$

In which w_E is the effective wake fraction, R_N the bare-hull resistance, t the thrust deduction factor and η_H and η_O are the hull efficiency and propeller open water efficiency respectively. η_{R} is the relative rotative efficiency, which for the present study is taken as 1.0.

Instead of w_E , the effective wake fraction, the nominal wake fraction w_N (which is obtained from the nominal calculation directly)

can be used instead. However, the nominal wake fraction may increase significantly in shallow water due to larger wake and possibly flow separation around the stern, following from increased pressure gradients. In an effective wake field, growth of the wake and flow separation are suppressed by the pressure decrease induced by the propeller. The velocities in the effective wake field are therefore higher than in a nominal wake field, and this difference between the nominal and effective wake field increases in shallow water (Kulczyk, 1970). Estimates of the nominal and effective wake fraction for a specific ship that was analyzed for the present study are presented in Table 2, showing that the difference increases while the nominal wake fraction grows significantly. A significant overestimation of the wake fraction in 1 leads to a too low power estimate. It is therefore important to use the effective wake field instead of a nominal wake field.

The effective wake field is obtained by subtracting the propeller-induced flow field from the wake field obtained from a total calculation (the total wake field). For determination, we apply a model based on actuator disk theory. In the model, two Bernoulli equations are applied: the first on the upstream side of the disk, the second downstream of the disk:

$$\begin{aligned} C_1 &= \frac{1}{2} \rho |u_1^x(x)|^2 + \rho g z_1 + p_1 \\ C_2 &= \frac{1}{2} \rho |u_2^x(x)|^2 + \rho g z_2 + p_2 \end{aligned} \quad (2)$$

where ρ is the fluid density, g the gravitational acceleration (9.81 m/s^2), $u_1^x(x)$ the flow velocity upstream of the disk, p_1 the pressure upstream of the disk and z_1 the vertical location of a fluid particle. The same applies for u^x , p and z with subscript 2. Fig. 5 gives a schematic overview of the flow through the disk with these symbols. At the disk, $z_1 = z_2$ and $u_1^x(x_{disk}) = u_2^x(x_{disk})$. Since the actuator disk induces a pressure jump in the flow, $C_2 = C_1 + \Delta p$. Far away from the disk however, p_2 is equal to p_1 and the pressure jump has been transformed in kinetic energy. Furthermore, assuming:

$$u^x(x_{disk}) = \frac{1}{2} (u_1^x(0) + u_2^x(\infty)) \quad (3)$$

It is possible to solve Eqs. (2) and (3). $u^x(x_{disk})$ is known from the total wake field, while Δp is known from the imposed thrust distribution. This leads to:

$$u_1^x(0) = \frac{|u^x(x_{disk})|^2 - 2\Delta p/\rho}{u^x(x_{disk})} \quad (4)$$

Eq. (4) is applied to each discrete element of the propeller disk by computing $\Delta p_i = F_i/(\Delta r \Delta \theta r)$. To finally obtain w_E , the average value of $u_1^x(0)$ is computed. Furthermore, η_O is obtained from Kaplan ducted propeller Series (Oosterveld, 1970), using a P/D ratio of 1.0 and $A_E/A_0 = 0.7$.

2.6. Surrogate modeling

From the experiment design and Parnassos computations, we obtain the power requirement for each tested hull form. Surrogate models are used to investigate quickly how the power requirement is affected by either hull form parameters as well as water depth, but also to compare optimization results for different water depths. A surrogate model is a model that replaces another model (in this case Parnassos), which usually computationally more expensive, to be able to quickly estimate the outcome of the expensive model at an untried location in the design space. Four different types of surrogate models are investigated:

- Quadratic response surface
- Kriging response surface
- Universal Kriging
- Radial Basis Function interpolation

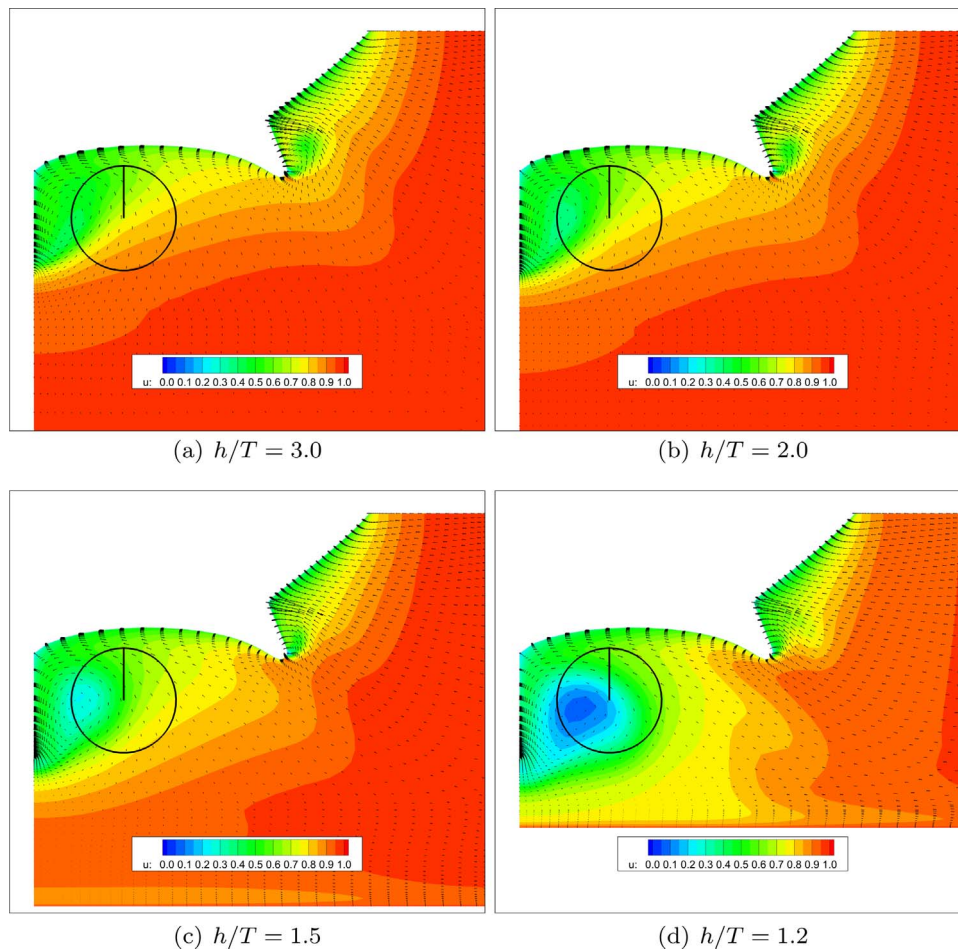


Fig. 6. Contour graph of longitudinal non-dimensional velocities ($u = u_x/V_5$) together with vectors indicating velocities in transverse directions, at four different water depths. The figures show that the ship wake grows significantly in shallow water, and the vectors that the flow becomes more horizontally oriented.

The quadratic response surface is a polynomial model of the form $\hat{y} = A + B_i x_i + C_i x_i^2 + D_{ij} x_i x_j$ (here, x_i represents a parameter value instead of a position). The coefficients for this polynomial are obtained using least-squares fitting. The Kriging response surface is a stochastic process that is formed from a correlation matrix and a series of fitted coefficients (Sacks et al., 1989). The universal Kriging model is a sum of the quadratic model and the Kriging response surface, such that the quadratic model fits the main trend while the (smaller) departures from that trend can be captured by the Kriging model. Finally, the Radial basis function interpolation model is a distance-based interpolation model.

Each of the models is tested using cross-validation. Furthermore, the models are tested using factor analysis, which is conducted as follows:

1. Start with a model with no parameters, only including the average value of power requirement across the dataset.
2. Try all available (not yet added) parameters for addition to the model
3. Add the parameter that resulted in the largest reduction of cross-validation error
4. With the model including the parameter added in 3, go back to 2 until all parameters are added.

This is similar to Analysis of Variance (ANOVA), but in ANOVA the effect of a parameter is represented by the change of the sum of squares explained by the model if a parameter is either removed or added. Since the sum of squares, as well as differences in the sum of squares for different models, can be very large, comparison between different

models is difficult. Furthermore, it is possible to notice over-fitting of the model (which occurs when the model includes too many parameters) since the cross-validation error will increase if too many parameters are in the model.

The Kriging models and the Radial basis model will, in general, fit all data exactly. This also includes the precise fitting of errors (numerical errors from CFD for example). As this is unfavorable, the used implementations include a smoothing parameter. This parameter allows the models to fit the data within a certain range around each data point. Using the smoothing parameter, the trends can be captured smoothly.

2.7. Optimization

In order to investigate whether there is a trade-off to be made between optimization for deep water or a specific water depth, a multi-objective (power estimates at different water depths) optimization procedure is used. For this, the NSGA-II algorithm (Deb et al., 2002) is applied, which is a genetic algorithm that allows testing of multiple objects and parameters. The algorithm searches for a Pareto front that contains a series of ship hull forms, each of which is optimal depending on the chosen trade-off between the included objectives.

For the present study, we perform two optimization studies, one for ship resistance and another one for required propulsion power. Optimization for resistance is included to show the impact of not including shallow water effects on wake fraction and thrust deduction in the power prediction and optimization. These effects have not yet been investigated thoroughly (Raven, 2016). In each optimization

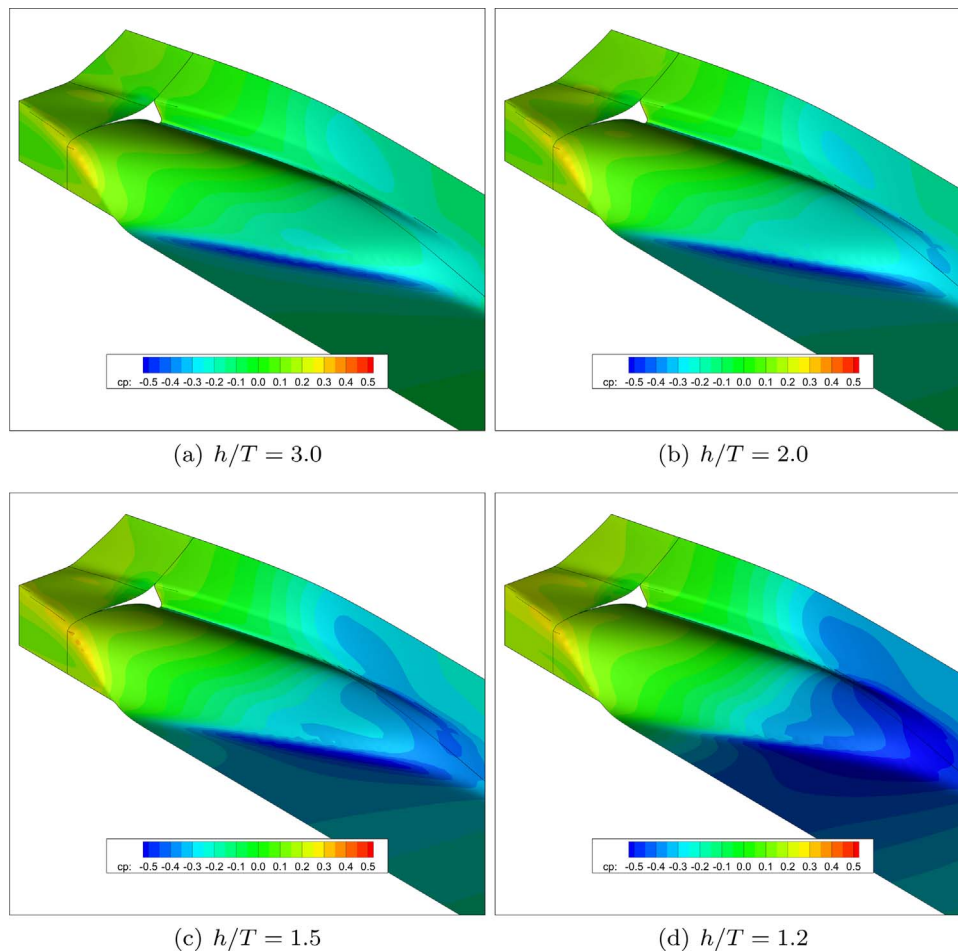


Fig. 7. Distribution of pressure coefficient, $(p - p_h)/0.5\rho V_S^2$ on the stern at four different water depths. The pressure drop around the aft shoulder significantly increases in shallow water. This leads to a stronger positive pressure gradient downstream of the shoulder, which can lead to separation.

study, the object functions applied are either resistance at two water depths or power at two water depths. The Pareto fronts obtained should then show whether it is important to take water depth into account in the optimization process of a ship hull.

The Pareto front is further analyzed to see which hull form parameters change along the front. This provides useful insight in how a ship can be optimized for shallow water. Furthermore, the change of resistance, wake fraction and thrust deduction is also investigated to see which of these parameters are a key influence in the trade-off between optimization at one or another water depth.

3. Results

This section discusses the computational results. First, the flow around the ship hulls is presented for different water depths and changes of several parameters. Next, the results are used to generate surrogate models and finally, these surrogate models are used to optimize the ship hulls for different water depths. Flow velocities and pressure are presented in a non-dimensional form. Velocities are made non-dimensional with ship speed, $u = u_x/V_S$. Pressures are presented using the dynamic pressure coefficient: $C_p = (p - p_h)/(1/2\rho V_S^2)$. For reference, graphs showing thrust deduction, nominal wake fraction and the resistance coefficients are presented in the appendix.

3.1. Flow analysis

In order to first present the effect that shallow water has on the flow around the ship, Fig. 6 shows a transverse cut of the flow near the

propeller position. The wake increases significantly in shallow water, while the flow also follows a more horizontal trajectory around the hull as indicated by the vectors. The changes are almost unnoticeable at $h/T = 2.0$, but become important at $h/T = 1.5$, although the most severe changes to the flow pattern occur at $h/T = 1.2$. Apart from the stronger wake and horizontally oriented flow, the figures also show that the vortex (indicated by the lower velocity area right of the tunnel skirt in each figure) shed from the tunnel skirt moves closer to the tunnel skirt and becomes smaller in shallow water for this specific hull form.

The significantly stronger wake in shallow water follows from the increase of pressure gradients around the stern. The pressure drop around the aft shoulder becomes stronger, while the pressure at the transom is larger. The following positive pressure gradient, which is larger than in deep water, slows down the flow around the stern, leading to the large wake.

Figs. 6 and 7 correspond to nominal calculations (i.e. without propeller effect) only. However, it is important that the limitations imposed by the river bottom also affect the effect that the propeller has on the pressure distribution around the ship. Fig. 8 shows the changes to the pressure distribution at the stern for four different water depths after the propeller effect was included in the calculations. Again, the effect is small at $h/T = 2.0$, but at $h/T = 1.5$ and lower, the pressure distribution is clearly affected. Noting that the propeller induces a pressure drop upstream of the propeller, the pressure gradients shown in Fig. 7 decrease. Therefore, the growth of the wake towards the propeller is suppressed. This underlines the importance of using the effective wake fraction in Eq. (1).

Fig. 9 shows the distribution of longitudinal velocity obtained from

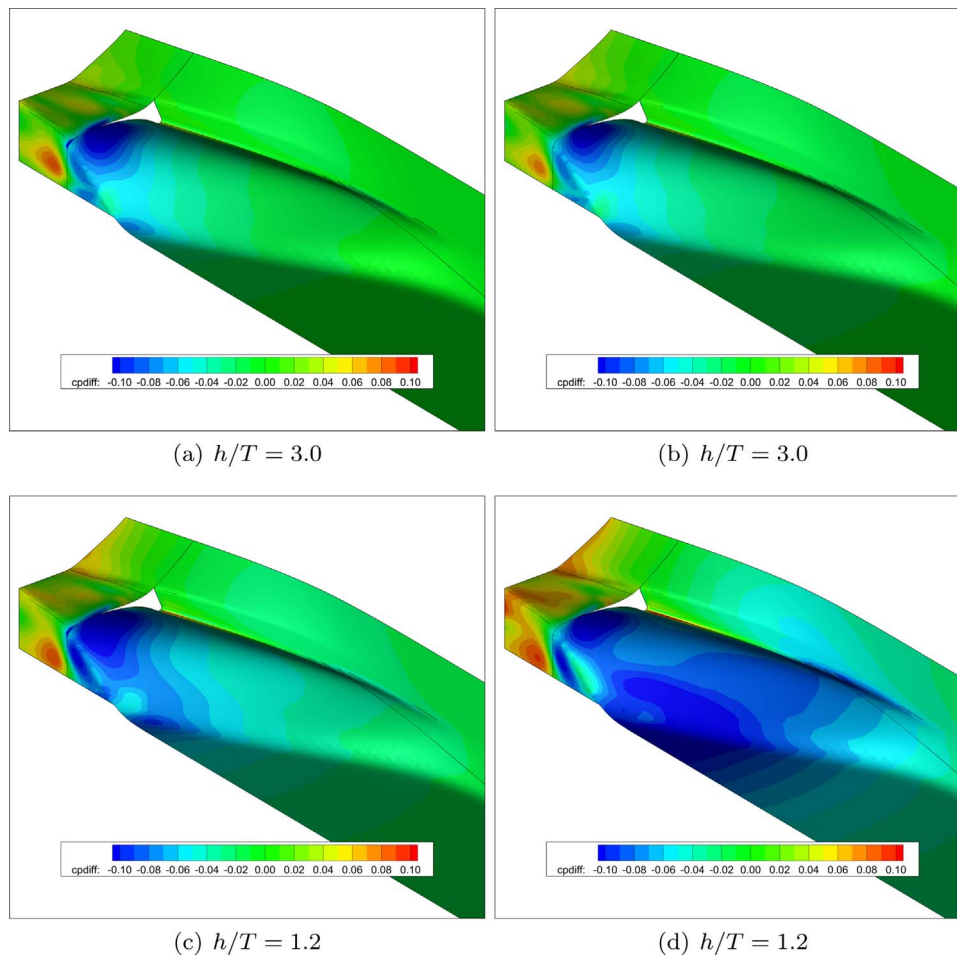


Fig. 8. Difference of the pressure coefficient distribution after activating the propeller at four different water depths. The propeller induces a pressure decrease upstream of the propeller, which leads to the thrust deduction effect but also lowers the pressure gradients in Fig. 7.

nominal calculations for two different ships, each at two different water depths. Similar to Fig. 6, the velocity deficit in the wake field increases in shallow water. Furthermore, if the propeller is positioned further away from the center, the velocity of the flow that passes through the propeller disk increases. At the tunnel skirt, the vortex being shed in deep water is smaller if the propeller (and therefore also the tunnel skirt) is located further away from the center. In shallow water, however, the vortex moves more towards the inside of the tunnel skirt due to a larger portion of the flow coming in from aside the ship compared to deep water, where more flow comes in from underneath the ship.

Fig. 10 shows similar data specifically for a change of the parameter V_{bottom} . For a V-shaped bottom, the velocity deficit in the wake field is larger.

Fig. 11 shows the effect of propeller action on the same ships as presented in Fig. 10, for two different water depths. The colors indicate the magnitude of local thrust deduction (i.e. the local propeller suction on the hull surface). It shows that the effect of thrust deduction increases in shallow water, and that the magnitude of thrust deduction on the ship hull is larger for the V-shaped bottom compared to the S-shaped bottom. Whereas Fig. 8 shows the pressure distribution, Fig. 11 shows the distribution of the local resistance contribution (which is obtained by multiplying the pressure with the x -component local surface normal and adding the local x -component of the shear force). The smaller effect on the resistance distribution is therefore explained by the fact that for an S-shaped bottom, the normals on the hull surface close to the propeller have a smaller component in longitudinal direction, leading to a smaller contribution of local pressure to the ship's resistance.

3.2. Surrogate modeling

Figs. 9, 10 and 11 already showed how parameters Y_{prop} and V_{bottom} influence the flow around the ship. In order to perform optimization, a surrogate model was created. The type of model to be used in optimization is selected based on cross-validation. Fig. 12 shows the cross-validation test for the four different models considered. The graph shows similar quality for the Kriging model, universal Kriging model and the quadratic model. The radial basis function (rbf) interpolation model yields larger errors.

Furthermore, the estimation of parameter influence as explained in Section 2 is applied to all models considered as well. Fig. 13 shows that for the Kriging models and the quadratic response surface, similar results are obtained expect for parameter V_4 (V_{top}). For V_{top} , the Kriging models show a larger influence whereas the other models show no influence at all. An explanation for this is that if the influence of that parameter does not follow a polynomial trend, the quadratic model - which is a second order polynomial function - can not capture it (for example, a sine-like effect with a period of half the design space width will be approximated as a constant by a quadratic model), while the Kriging models are able to capture such behavior.

From Figs. 12 and 13, the quadratic response surface is chosen as the model for the remainder of the study. The reasons for this are that the quadratic model is relatively simple, its estimates of parameter influence for the most important parameters are similar to those from other models and the model is relatively insensitive to errors in the data. The Kriging models on the other hand, in general will fit all data as close as the error parameter allows. It can therefore be more

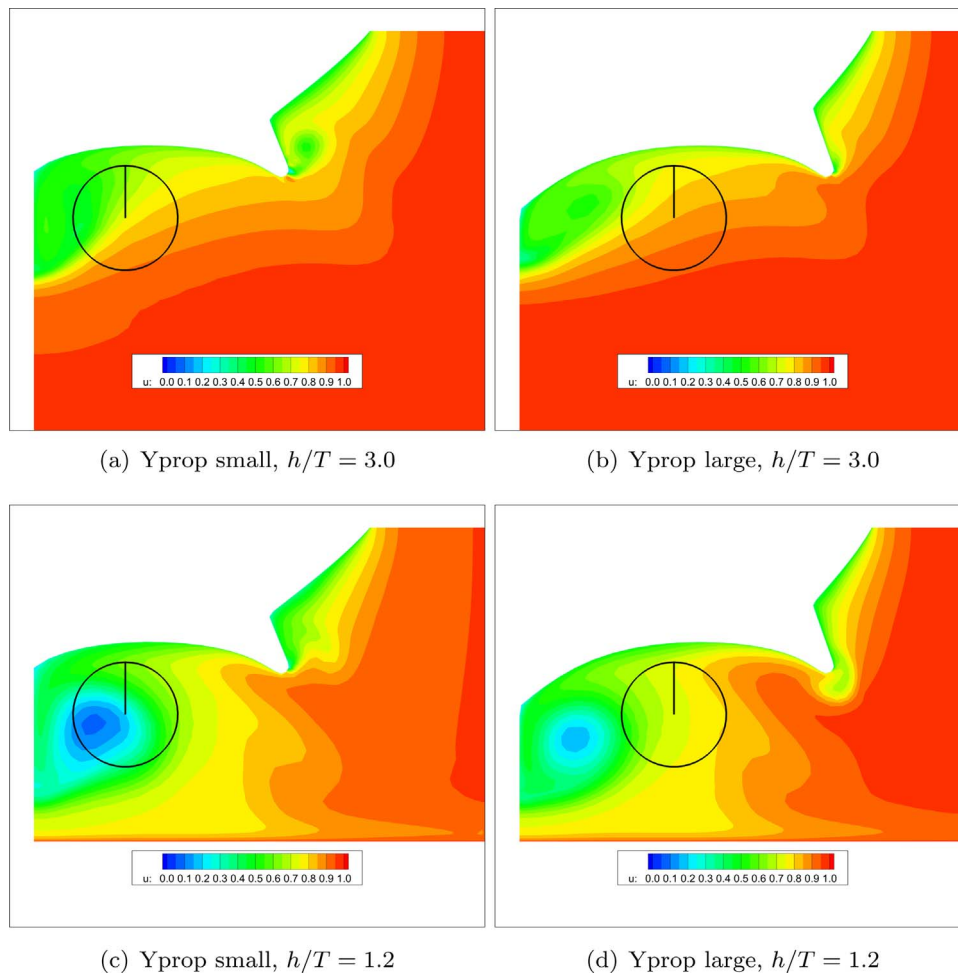


Fig. 9. Contour graph of longitudinal - nominal - velocity at the propeller position. for different Y_{prop} values, showing that for a lower Y_{prop} value, the propeller operates in a stronger wake.

accurate, but if a data point is further away from the general trend than the chosen error parameter would allow, the Kriging models may show off-trend behavior around such a point. Therefore, the robustness of a quadratic model is favored over the accuracy of a Kriging model for this study. The radial basis function interpolation is not used because it showed the largest errors for the cross-validation test.

As stated in Section 2, 8 points that were randomly spread across the design space had to be removed from the dataset. To test the effect of removing these points, up to 10 randomly chosen additional points are removed from the data set, while measuring the quality of the data set using 5-fold cross-validation for a fitted regression model. This process is repeated 10,000 times. Fig. 14 shows the (increasing) cross-validation error of a regression model fitted to the results at $h/T = 3.0$. Both the maximum error and 95th percentile of the errors are shown. This last one is a useful measure of the impact of point removal. The first, the maximum error, occurs if the removed points are all in the same area of the design space. Both values, however, are well within the variational range of propulsion power (60 kW).

The quality of the chosen response surface with regard to data representation is shown in Fig. 15. Cross-validation results are presented for the four water depths considered. As shown in the results, the model is well able to represent the data.

Fig. 16 shows how the amount of variation not explained by the model decreases (i.e. how the model's data representation capability increases) when parameters are added. In all cases, most of the variation is explained by the first two parameters, being Y_{prop} and V_{bottom} respectively.

The results from Fig. 16 can also be shown in a way that directly

shows the influence of each parameter on the model. This is obtained by taking the differences between subsequent points in the graphs in Fig. 16, and plotting these values in Fig. 17.

An important observation that can be made from Fig. 17 is that the influence of V_{bottom} (V_2 in the figure) increases when water depth decreases. This follows from the effect that V_{bottom} has on the ship hull: it moves the surface of the ship hull closer to, or further away from the propeller. Thereby, it affects the thrust deduction factor, which increases for decreasing water depth, as shown in Fig. 11.

3.3. Optimization

Optimization is conducted using the surrogate models generated from the data. The genetic algorithm NSGA-II is applied. The results are shown in Fig. 18. The NSGA-II algorithm processes multiple generations. The colors of the dots move from blue to red if the dots belong to younger generations. The figure shows a clear Pareto front if propulsion power predictions at $h/T = 3.0$ and $h/T = 1.2$ are used as objectives. In cases where optimization is conducted for power prediction at $h/T = 3.0$ and $h/T = 2.0$, or for those at $h/T = 3.0$ and $h/T = 1.5$, the Pareto front is less clear. For the rightmost graph in Fig. 18, the Pareto front shows that if solely optimizing for power at $h/T = 1.2$ (vertical axis), propulsion power at deep water ($h/T = 3.0$, horizontal axis) would increase by approximately 5 percent.

To address the importance of optimizing for power - which involves propulsion parameters that also change in shallow water - Fig. 19 presents the optimization of the ship hull for resistance only. The Pareto fronts are smaller than those in Fig. 18, if not entirely absent.

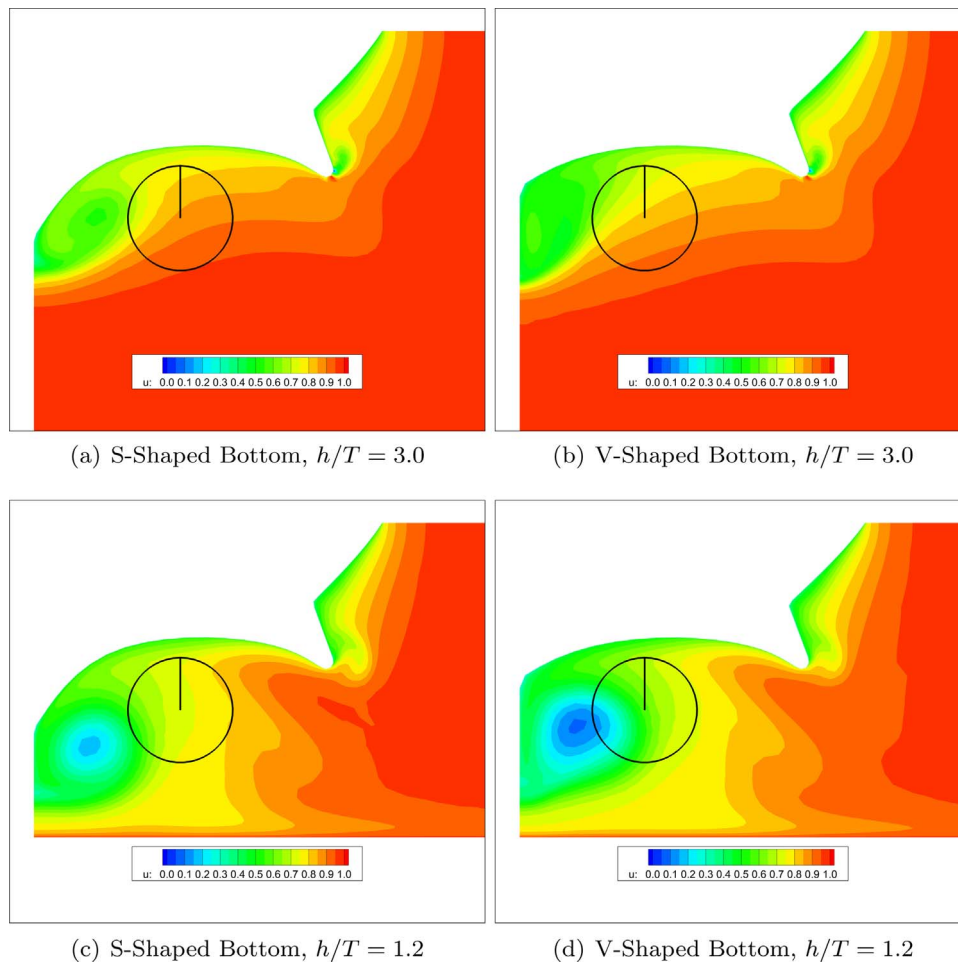


Fig. 10. Flow visualization for different V_{bottom} values, showing a stronger wake field for the V-shaped bottom.

This indicates that if the ship is only optimized with respect to resistance, taking water depth into account does not affect the optimal hull shape for the design space considered (i.e., the optimal ship in deep water is still the optimal ship in shallow water).

Prior publications (Zhao, 1984; Saha et al., 2004) that show a different optimal ship for another water depth if only focusing on resistance, took wave resistance into account. For the low Froude numbers relevant to inland ships however, the wave resistance is only a small portion of the total resistance. Therefore, it is not expected that including free-surface effects would significantly change the outcomes of the presented optimization study.

The existence of the Pareto front in Fig. 18 indicates that one or more parameters change if optimization is performed for one water depth or another. Fig. 20 therefore shows which parameters are changing along the Pareto front. The parameter that changes is V_2 (V_{bottom}). Furthermore, the value of Y_{prop} (V_1) is always 1.0, such that the propeller is close to the ship centerline. R_{bilge} is not presented in Fig. 20, because it has a negligible influence on the estimation of propulsion power as shown in Fig. 16. V_{top} is always 1.0, such that the tunnel top curve is always in alignment with the propeller shaft. The effect of V_{top} on the prediction of propulsion power is small, however, as shown in Fig. 17.

4. Analysis and discussion

In the parameter analysis, it is clear that for deep water, Y_{prop} (V_1) is the most relevant parameter to the power requirement of the ship. We can also see this in Fig. 9, which shows that in case of a smaller

Y_{prop} value, the propeller moves into a stronger wake field, which leads to increased hull efficiency (η_H). In shallow water however, V_{bottom} (V_2) becomes more important as presented in Fig. 17. The influence of R_{bilge} (V_3) decreases if the water depth decreases, and the influence of V_{top} (V_4) is small or even negligible in any water depth considered.

The increasing influence of V_{bottom} when the water depth decreases can be explained using Fig. 10. For two ships with a different bottom shape, the difference in the wake field is small at $h/T = 3.0$. At $h/T = 1.2$ however, the wake fields of both ships differ significantly. Furthermore, Fig. 11 shows that the extent of the propeller induced resistance becomes larger in shallow water, and the bottom shape has a strong influence on the part of the stern where the pressure distribution is affected the most by suction of the propeller.

That the influence of R_{bilge} decreases in shallow water is due to the fact that flow comes in from aside the ship rather than from underneath. Therefore, the flow does not have to pass the bilge, which in deep water leads to vortices being shed. These vortices are also present in shallow water, but they do not significantly depend on R_{bilge} .

Fig. 18 shows that there is a trade-off between optimization for deep water and optimization for shallow water. Since the horizontal axis shows the percentage of power at $h/T = 3.0$ relative to the mean value, and the vertical axis does so for water depths at $h/T = 2.0$, 1.5 and 1.2, a decrease of approximately 5 percent of power can be achieved for $h/T = 1.2$, if a 5 percent increase of power in deep water is accepted. For water depths at $h/T = 2.0$ and $h/T = 1.5$, this trade-off is much smaller. It is therefore important that already during the design process, water depths that will be encountered by the ship are

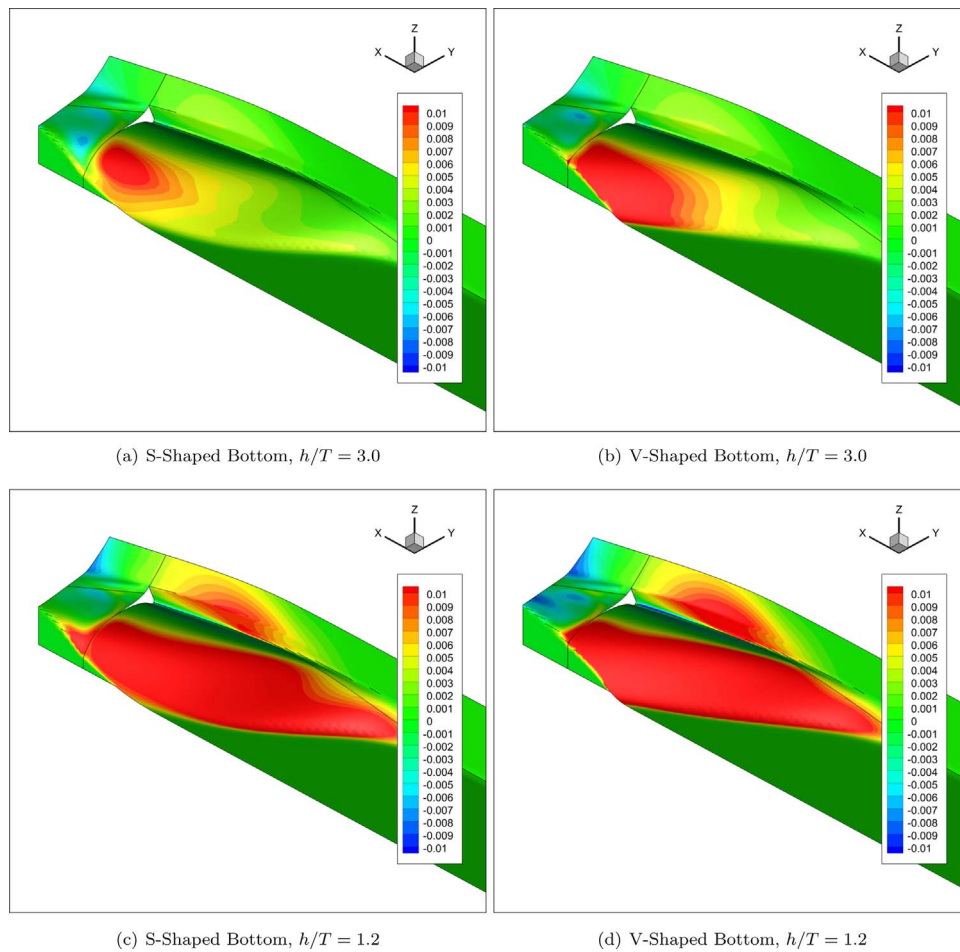


Fig. 11. Distribution of the thrust deduction effect on resistance, for two ships that mostly differ for their bottom shape.

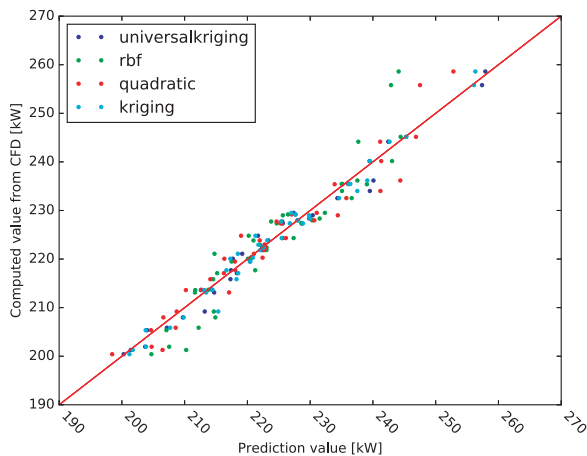


Fig. 12. Cross-validation for the estimation of power, for each of the model types considered. The horizontal distance from the straight line indicates how close the prediction is to the value computed from CFD.

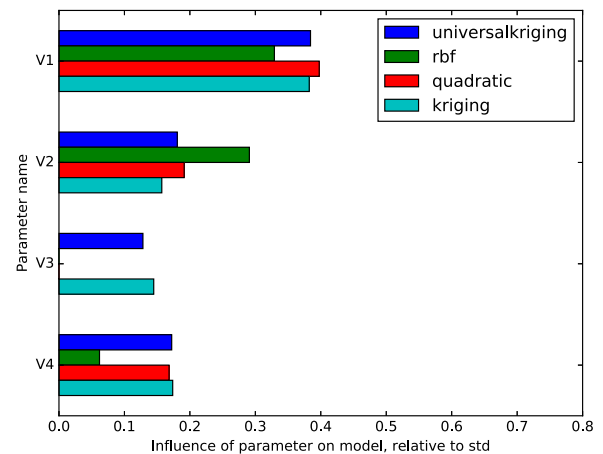


Fig. 13. Parameter influence on the estimation of power, for each of the model types considered. The parameter influence is normalized with the standard deviation in the data (std).

taken into account. If h/T ratio lower than 1.5 are frequently encountered, optimization for water depths corresponding to those h/T ratio can prove beneficial. On the other hand, if the ship is expected to mostly encounter h/T ratios larger than 1.5, effects of shallow water do not affect the optimization of the stern significantly. Furthermore, the figures show that optimization for resistance only is not sufficient: the trade-off is significantly smaller than that for propulsion power.

This is due to effects of shallow water on wake fraction and thrust deduction (which can be observed in Figs. 9, 10 and 11), on top of those on resistance. This is important and shows the need for further research into the field of shallow water propulsion parameters as available knowledge on that is lacking Raven (2016).

The increasing influence of V_{bottom} in shallow water, observed from Fig. 17, is reflected by the ships that lie at the Pareto front in

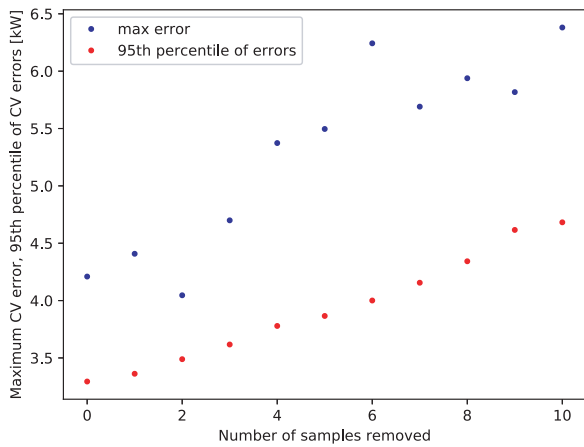


Fig. 14. Regression model cross-validation (CV) error upon removal of points from the dataset. The maximum CV error and the 90th percentile of CV errors are presented. The total range of variation is 60 kW.

Fig. 18. The value of V_{bottom} (V_2) decreases when the ship is optimized for shallow water (thus increased deep water power in Fig. 20), meaning that the bottom should become V-shaped in shallow water, while a slightly more S-shaped bottom is favorable in deep water. This is due to the fact that in shallow water, the V-shaped bottom yields a stronger wake, which is favorable for hull efficiency. In deep water, the differences between the two wake fields are smaller (see Fig. 10), but the increased resistance following from the fuller V-shaped bottom here causes the optimization algorithm to favor an S-shaped stern.

Parameters Y_{prop} (V_1) and R_{bilge} (V_3) are constant along the Pareto front: In any case, situating the propeller closer to the ship center yields a stronger wake field and therefore larger hull efficiency.

This results in lower propulsion power. This underlines the need to optimize for power instead of resistance, as situating the propeller closer to the ship center will lead to increased resistance (Rotteveel and Hekkenberg, 2015). R_{bilge} is always around the value of 0.8: it was expected to be at 1.0 as the largest bilge radius results in less vortices being shed and therefore less resistance. This is due to the fact that the fitting approach for the quadratic response surface minimizes the average value of summed squared errors between data points and predictions (least-squares fitting). Since it is the average value that is minimized, errors in certain areas of the design space can increase if in that case errors in other areas decrease more, achieving a lower error average. This may especially affect the behavior of parameters with a relatively low influence on the predictions, or in regions where the parameter is near its optimal value (in such a region, the prediction does not change significantly if the parameter value changes). Another conclusion applies as well: apparently, further increasing the parameter R_{bilge} does not lead to a significant decrease of the power requirement. Otherwise, the errors between the predictions and the data from CFD would have been larger.

Parameter V_{top} (V_4) is at the maximum value in general, which means the tunnel top curve is aligned with the tunnel skirt. However, once V_{bottom} reaches the minimum value and the bottom is V-shaped, V_{top} starts to decrease. It is important to note, however, that the influence of V_{top} on the power prediction is negligible, as seen in Fig. 17. The effect of the decrease is negligible, and occurs because the genetic algorithm aims to find the absolute minimum of the response surface within the design space. If other parameters are at the borders of their range, and any further decrease - although small - can be achieved, it will change other parameters as well. Hence, one should be careful with drawing conclusions on the V_{top} parameter from graphs such as Fig. 20.

That other parameters are at the border of their range implies that further improvements may be possible if the parameter range is widened. However, in case of Y_{prop} for example, further moving the

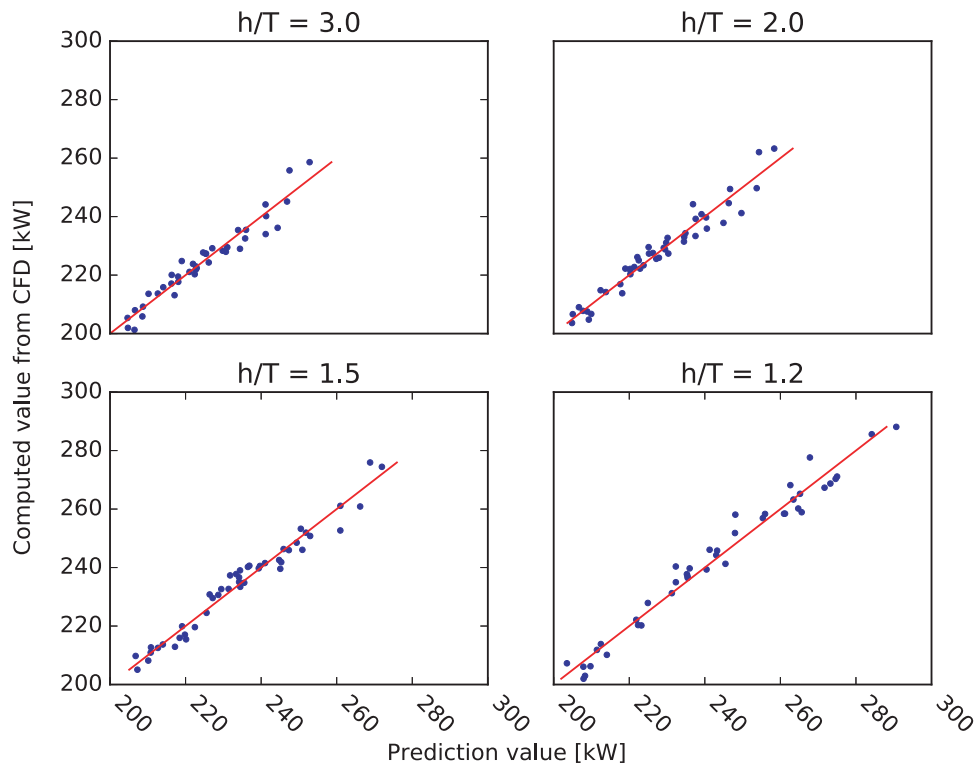


Fig. 15. Cross-validation for the estimation of power using quadratic response surfaces. All predictions are within 4 percent of the value computed from the CFD result.

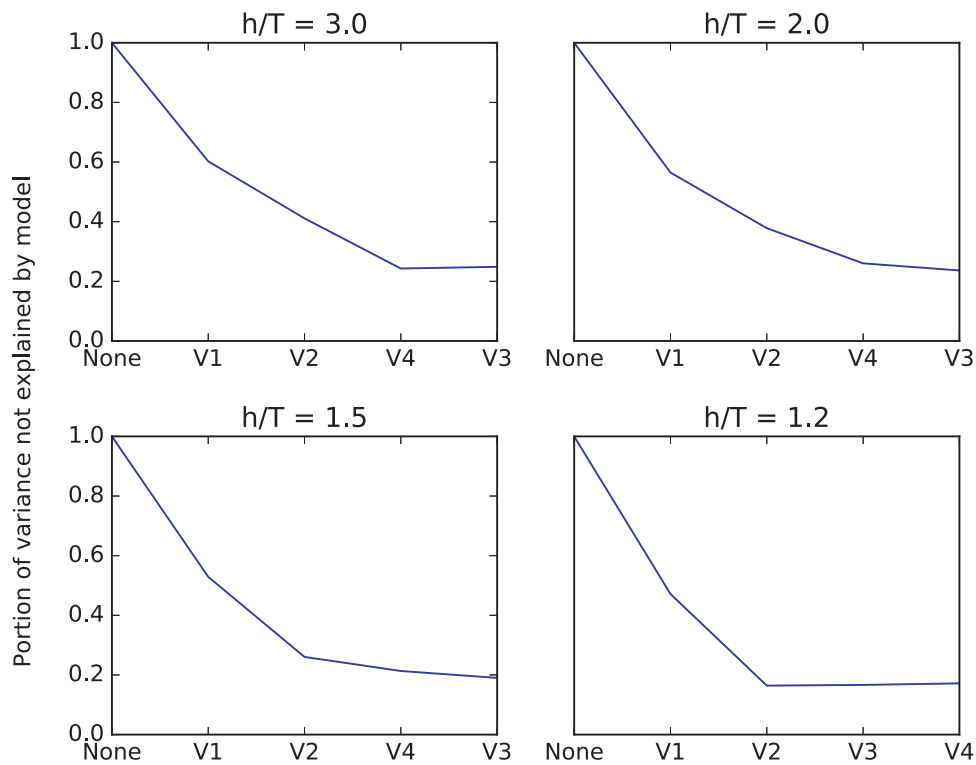


Fig. 16. Effect of adding parameters to the power prediction response surface for different water depths. The first two parameters, V1 and V2, respectively Y_{prop} and V_{bottom} , explain most of the variation in the models. Note that because each parameter addition leads to a better approximation of the data, the vertical axis shows the amount of error *not* explained by the model. From $h/T = 3.0$ to $h/T = 1.2$, it can be observed that the influence of V4 (V_{top}) decreases. In very shallow water is equally (un)important as V3 (R_{bilge}). In fact, adding V4 (V_{top}) to the model even has a small negative impact on the amount of explained variation. Therefore, V4 is added later to the model in case $h/T = 1.2$.

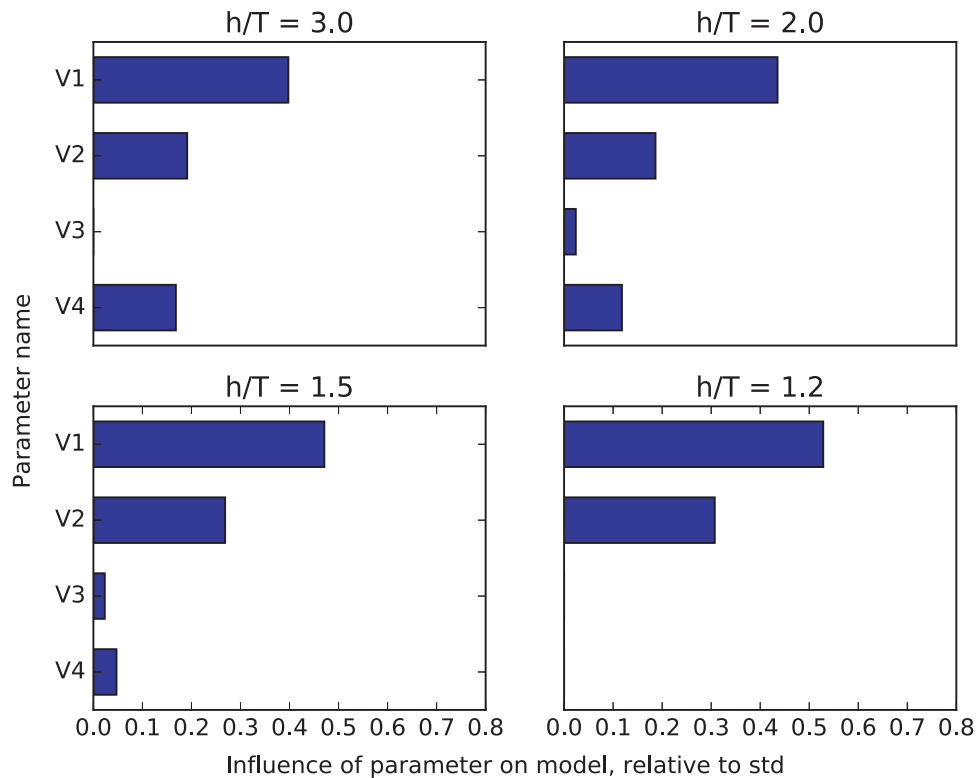


Fig. 17. Influence of each of the parameters on the power prediction quadratic response surface. In water of less depth, the influence of V_{bottom} (represented as V2 here) becomes larger, while effects of V3 and V4 diminish. Again, parameter influence has been normalized with the standard deviation (std) in the data.

propeller towards the ship center would be unfeasible since either the wake field will be of too low quality, or the two propellers will interfere with each other or hit the hull surface. The optimization algorithm does

not take feasibility into account and will therefore try to put the propeller position as close as possible to the ship center, since that increases the wake fraction and will therefore decrease the power

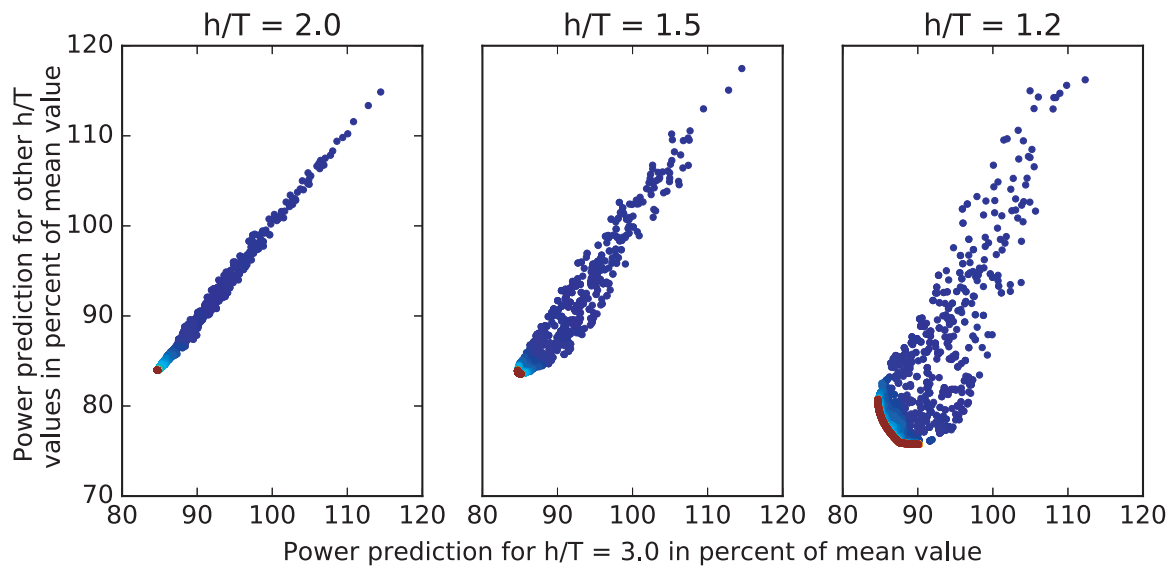


Fig. 18. Optimization of the ship hull where the objects are the propulsion power estimates at two different water depths. The values on the axis are relative to the mean value of data in the corresponding surrogate models. The Pareto front can be identified, especially for the case where the power at $h/T = 1.2$ is optimized against that for $h/T = 3.0$ (rightmost graph).

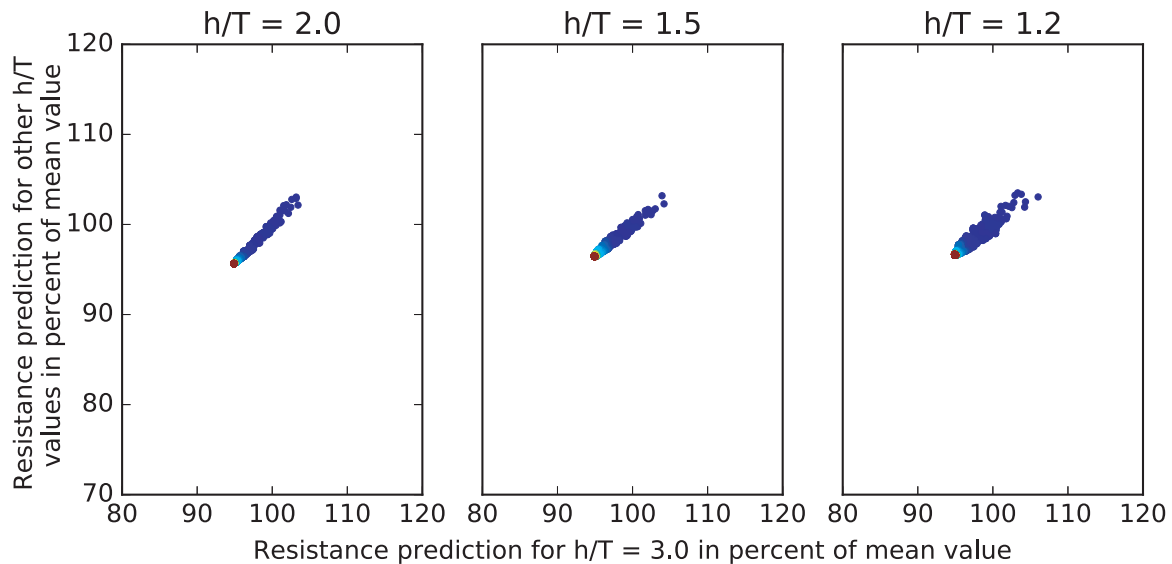


Fig. 19. Optimization of the ship hull for resistance at different water depths. The values on the axis are relative to the mean value of data in the corresponding surrogate models. The Pareto fronts are smaller than observed in Fig. 18, where optimization is presented for propulsion power.

requirement. The parameter ranges have therefore been chosen such that the design space only includes realistic hull forms.

A note should be made, however. One is that the used propeller model - an actuator disk - is not affected by the quality of the wake field. Hence, a stronger wake field - whether the velocity distribution is close to uniform or heavily fluctuating - always leads to a decrease of the power requirement. In reality, a low wake quality with large changes of inflow velocity across the propeller disk can increase the risk of cavitation and vibrations. Another note concerns the estimation of the effective wake field: the current actuator disk theory based approach only addresses longitudinal flow. Although this is the largest contribution to the wake fraction, part of the propeller thrust will in reality convert transverse flow into longitudinal flow, which in this case leads to a slightly incorrect estimation of the effective wake fraction. Despite this, the observed trends among the ships are expected to hold per water depth, since the variation of Y_{prop} is not such that large variations of the transverse flow contribution on the wake fraction can

be expected. Between water depths, the contribution of transverse flow to the wake fraction may change. The optimization results still hold as those are performed per water depth.

5. Conclusions

This paper presents an optimization study of an inland ship hull form with four shape parameters. The Parnassos RANS Solver has been used to obtain results for a series of hull forms. Then, surrogate models have been generated and used to analyze the influence of the parameters and to optimize the hull form for different water depths. From this study, the following conclusions are drawn:

- In different water depths, other parameters are important to the power prediction. In this study, the importance of the bottom shape increased in shallow water.
- A decrease of power requirement in shallow water can be achieved if

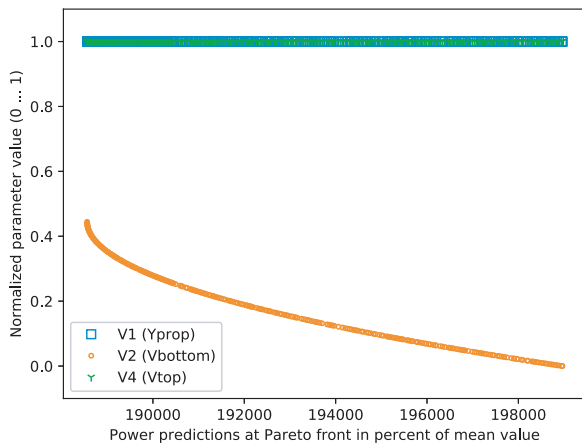


Fig. 20. Values of hull form parameters of ships that lie on the Pareto front in Fig. 18. The horizontal axis depicts the power estimate in deep water. Therefore the estimated amount of required power in shallow water decreases from left to right. The figure shows that along this Pareto front, Vbottom (V2) varies most. Hence, this parameter is subject to a trade-off in optimization for one water depth or another.

optimization is conducted at that water depth rather than in deep water. In this case, a five percent decrease of power was achieved in shallow water ($h/T = 1.2$) at the cost of a five percent power increase in deep water ($h/T = 3.0$).

- Optimization for resistance only is not sufficient. Compared to optimization for power, parameters obtain different optima and

trends along Pareto fronts may be opposite.

- Given the current set of parameters involved, the propellers should be situated close to the center plane in any water depth.
- In shallow water, the bottom should be V-shaped in order to minimize the power requirement. In deep water, the favorable bottom shape changes to an S-shape.
- For optimization of propulsion power, water depth should be taken into account if the h/T ratio is below 1.5 for the parameters currently considered.

For further study, more parameters and a wider range for the currently used parameters could be included in the analysis. Also, the results show that the effects of shallow water on w_E and t are significant. Apart from w_E and t , the relative rotative efficiency η_R might also change due to different flow behavior in shallow water. Since there are no easily applicable models available to estimate effects of shallow water on wake fraction and thrust deduction, and the research into this field is limited, investigation of shallow water effects on propulsion rather than resistance is advised.

Acknowledgments

The research presented was performed as part of the Joint Industry Project: Top Ships. In this project, a group of Dutch Ship Designers involved in the design and operation of inland ships provided funding for research to achieve better guidelines and knowledge regarding inland ship hull form design.

Appendix

Figs. A1 and A2

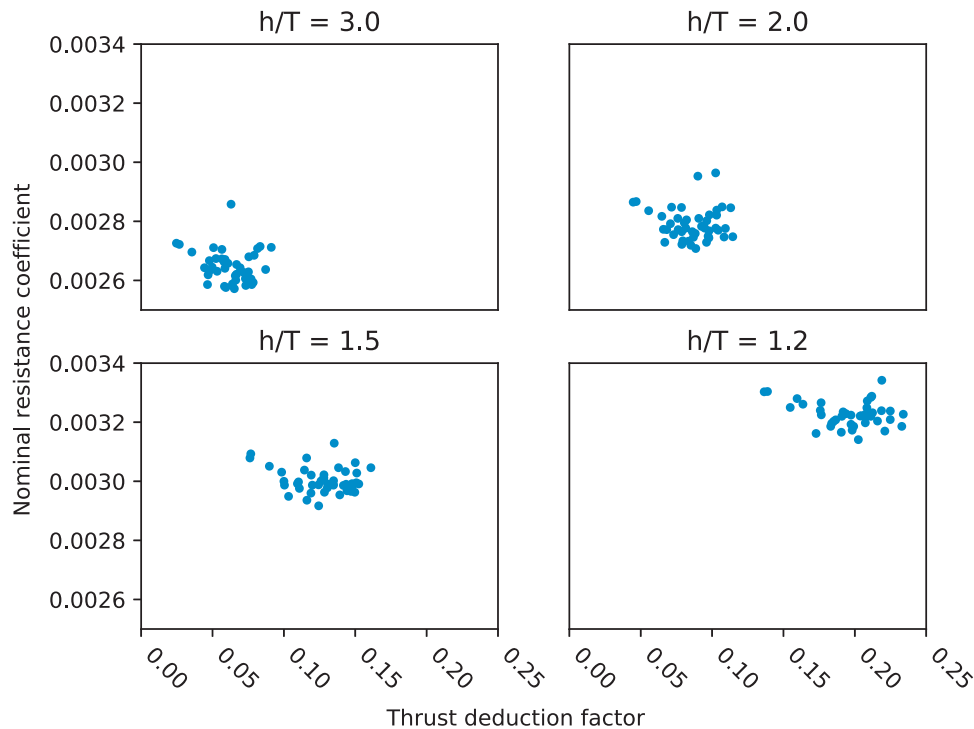


Fig. A1. Nominal resistance coefficient ($R_N/(0.5\rho V_S^2 S)$) versus deduction factor for all ships at four different h/T ratios.

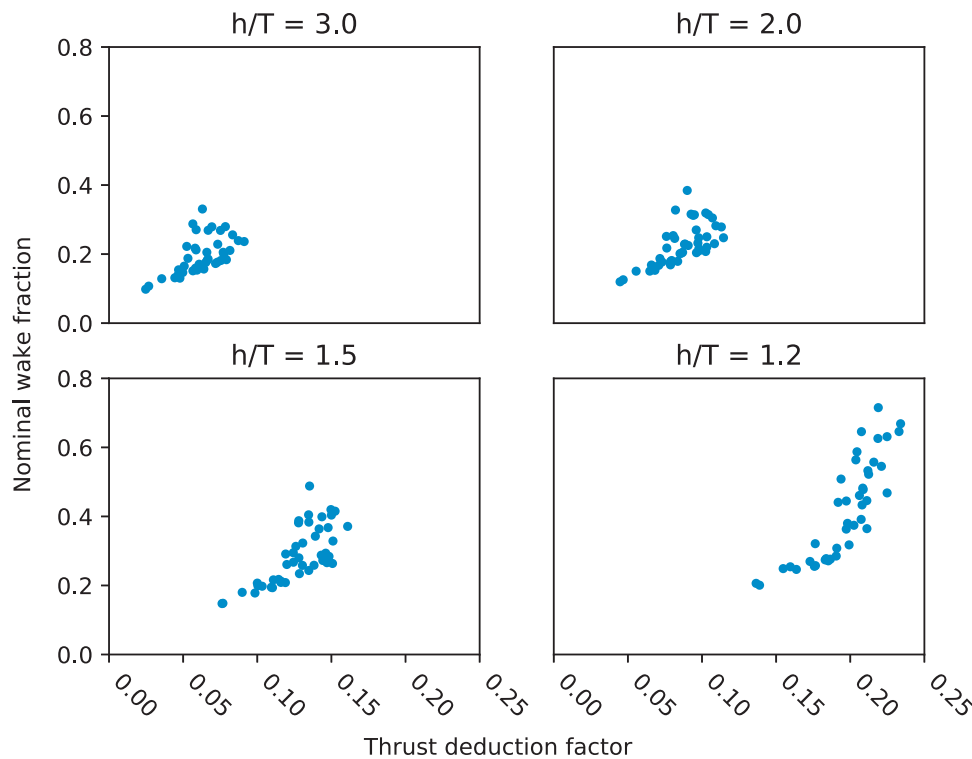


Fig. A2. Nominal wake fraction versus deduction factor for all ships at four different h/T ratios.

References

- Deb, K., Pratap, A., Agarwal, S., Meyarivan, T., 2002. A fast and elitist multiobjective genetic algorithm: Nsga-II. *IEEE Trans. Evolut. Comput.* 6, 182–197. <http://dx.doi.org/10.1109/4235.996017>.
- Eça, L., Hoekstra, M., 2014. A procedure for the estimation of the numerical uncertainty of cfd calculations based on grid refinement studies. *J. Comput. Phys.* 262, 104–130. <http://dx.doi.org/10.1016/j.jcp.2014.01.006>.
- Ferreiro, L.D., 1992. The effects of confined water operations on ship performance: a guide for the perplexed. *Nav. Eng. J.* 104, 69–83, (<http://dx.doi.org/10.1111/j.1559-3584.1992.tb01784.x>).
- Harvald, S.A., 1977. Wake and thrust deduction at extreme propeller loadings for a ship running in shallow water. *RINA Suppl. Pap.*, 119.
- Hoekstra, M., 1999. Numerical simulation of ship stern flows with a space-marching Navier-Stokes method. TU Delft, Delft University of Technology.
- Kulczyk, J., 1970. Propeller-hull interaction in inland navigation vessel. *WIT Trans. Built Environ.*, 12.
- Lackeny, H., 1963. The effect of shallow water on ship speed. *Shipbuild. Mar. Eng.* 70, 446–450.
- Menter, F.R., 1997. Eddy viscosity transport equations and their relation to the $k-\epsilon$ model. *J. Fluids Eng.* 119, 876–884. <http://dx.doi.org/10.1115/1.2819511>.
- Oosterveld, M.W.C., 1970. Wake adapted ducted propellers. Ph.D. thesis TU Delft, Delft University of Technology.
- Raven, H., 2012. A computational study of shallow-water effects on ship viscous resistance. In: *Proceedings of the 29th Symposium on Naval Hydrodynamics*, Gothenburg.
- Raven, H., 2016. A new correction procedure for shallow-water effects in ship speed trials. In: *Proceedings of the 2016 PRADS Conference*, Copenhagen.
- Rotteveel, E., Hekkenberg, R., 2015. The influence of shallow water and hull form variations on inland ship resistance. In *IMDC 2015: Proceedings of the 12th International Marine Design Conference*, Tokyo, Japan, 11–14 May 2015.
- Sacks, J., Schiller, S.B., Welch, W.J., 1989. Designs for computer experiments. *Technometrics* 31, 41–47. <http://dx.doi.org/10.1080/00401706.1989.10488474>.
- Saha, G.K., Suzuki, K., Kai, H., 2004. Hydrodynamic optimization of ship hull forms in shallow water. *J. Mar. Sci. Technol.* 9, 51–62. <http://dx.doi.org/10.1007/s00773-003-0173-3>.
- Schlichting, O., 1934. *Schiffwiderstand auf beschränkter wassertiefe: widerstand von seeschiffen auf flachem wasser*. *Jahrb. der Schiffbautech. Ges.* 35, 127.
- Tuck, E., 1978. Hydrodynamic problems of ships in restricted waters. *Annu. Rev. Fluid Mech.* 10, 33–46. <http://dx.doi.org/10.1146/annurev.fl.10.010178.000341>.
- Van der Ploeg, A., Starke, B., 2013. Prediction of the transom flow regime with viscous free surface computations. In *MARINE 2011, IV International Conference on Computational Methods in Marine Engineering*, pp. 261–272. Springer.
- Van der Ploeg, A., Eça, L., Hoekstra, M., 2001. Combining accuracy and efficiency with robustness in ship stern flow computation. In: *Proceedings of the Twenty-Third Symposium on Naval Hydrodynamics*.
- Zhao, L.-e., 1984. Optimal ship forms for minimum total resistance in shallow water. *Schr. Schiffbau*, 445. <http://dx.doi.org/10.15480/882.930>.